The Astrophysical Journal Letters, 876:L13 (3pp), 2019 May 1 https://doi.org/10.3847/2041-8213/ab1b0d

Line Ratios Reveal N_2H^+ Emission Originates above the Midplane in TW Hydrae

Kamber R. Schwarz[1,3], Richard Teague[2], and Edwin A. Bergin[2]

[1] Lunar and Planetary Laboratory, University of Arizona, 1629 East University Boulevard, Tucson, AZ 85721, USA; kschwarz@lpl.arizona.edu

[2] Department of Astronomy, University of Michigan, 1085 South University Avenue, Ann Arbor, MI 48109, USA

Received 2019 February 21; revised 2019 April 16; accepted 2019 April 18; published 2019 May 3

Abstract

Line ratios for different transitions of the same molecule have long been used as a probe of gas temperature. Here we use ALMA observations of the N_2H^+ $J = 1$–0 and $J = 4$–3 lines in the protoplanetary disk around TW Hya to derive the temperature at which these lines emit. We find an averaged temperature of 39 K with a 1σ uncertainty of 2 K for the radial range $0\farcs8$–$2''$, which is significantly warmer than the expected midplane temperature beyond $0\farcs5$ in this disk. We conclude that the N_2H^+ emission in TW Hya is not emitting from near the midplane, but rather from higher in the disk, in a region likely bounded by processes such as photodissociation or chemical reprocessing of CO and N_2 rather than freeze-out.

Key words: astrochemistry – ISM: molecules – protoplanetary disks – techniques: interferometric

1. Introduction

In protoplanetary disks molecular line emission is used to obtain the abundances of different species as well as measure physical properties within the disk such as temperature, turbulence, and ionization. One species that has proved useful for constraining physical properties is N_2H^+, a molecular ion that emits strongly in protoplanetary disks. N_2H^+ is formed when H_3^+ transfers a proton to N_2 and is destroyed primarily by reacting with CO. Because of this, as well as the formation reaction competing with proton transfer between H_3^+ and CO, N_2H^+ only exists at large abundances in regions with N_2 gas but without a large CO gas abundance. As such, N_2H^+ is a potential tracer of the CO snowline (Qi et al. 2013).

For rings of N_2H^+ emission the inner radius of the emission has been posited to trace the midplane CO snowline for TW Hya and HD 163296. For HD 163296 the CO snowline location based on N_2H^+ emission is in good agreement with the snowline location as determined by $C^{18}O$ observations (Qi et al. 2015). However, for TW Hya the snowline location of 30 au based on N_2H^+ emission is significantly farther out than the midplane snowline location of 17 au derived from observations of $^{13}C^{18}O$ (Qi et al. 2013; Zhang et al. 2016). Additionally, N_2H^+ emission does not appear to trace the CO snowline in the V4046 Sgr disk (Kastner et al. 2018).

Using physical–chemical and radiative transfer modeling, van't Hoff et al. (2017) argued that this discrepancy is due in part to some of the N_2H^+ emission originating from higher in the disk. The utility of N_2H^+ as a snowline tracer thus depends on the physical properties of the protoplanetary disk, including its temperature structure. In this Letter we use the ratio of N_2H^+ $J = 4$–3 to N_2H^+ $J = 1$–0 emission observed in TW Hya to derive the average temperature of the N_2H^+ emitting ring. We demonstrate how temperatures derived from line ratios can inform our understanding of the likely formation pathway of a given molecule, as well as what underlying conditions gave rise to the morphology of the emitting region.

[3] Sagan Fellow.

2. Observations

The Atacama Large Millimeter/submillimeter Array (ALMA) Band 3 observations targeting N_2H^+ $J = 1$–0 where obtained on 2016 October 2 with 42 antennas as part of project 2016.1.00592.S (PI: K. Schwarz). The data were calibrated and imaged using `CASA v4.7.0`. Phase and amplitude self-calibration were performed on the continuum and applied to the line spectral window. Continuum subtraction was performed using the `CASA` task `uvcontsub`. The line data were imaged using natural weighting, resulting in a $0\farcs62 \times 0\farcs49$ beam and a per channel rms noise level of 2.2 K per 0.1 km s^{-1} channel. Additionally, we use archival observations of the N_2H^+ $J = 4$–3 transition (2011.0.00340.S, PI: C. Qi). For a detailed discussion of the data reduction we refer the reader to Qi et al. (2013). Here we report only the properties of the final N_2H^+ image cube for comparison with the 1–0 data. The final image has a synthesized beam of $0\farcs63 \times 0\farcs59$ and a per channel rms noise level of 0.71 K per 0.1 km s^{-1} channel.

3. Analysis

After standard calibration, emission from the N_2H^+ $J = 1$–0 transition is not apparent in either the channel maps or moment 0 map. The lack of direct detection of the 1–0 transition in the image plane gives an upper limit on the integrated line intensity of 2.7 K km s^{-1} for a single hyperfine component, where the upper limit is rms $\times \sqrt{N_{\rm chan}} \times \delta v$ and $\delta v = 1.5$ km s^{-1} is the line width based on the 4–3 data. The upper limit for the seven hyperfine components added in quadrature is then 7.1 K km s^{-1}. In order to improve the signal-to-noise ratio (S/N) of the spectra we employ the stacking method for Keplerian disks introduced by Yen et al. (2016). Using the package `eddy` (Teague 2019) the image cube is divided into concentric annuli, which are each de-projected to the system velocity assuming the physical and kinematic properties derived from previous analysis of the CS emission in TW Hya (Teague et al. 2018). The de-projected spectra are then stacked. Line emission is weakly detected in the annular bins in the range $0\farcs8$ to $2''$ from source center. In comparison, bright N_2H^+ 4–3 emission is observed in the image plane in a ring from $0\farcs8$ to $1\farcs2$, though weaker emission can be seen out to $2\farcs5$ (Qi et al. 2013). Figure 1 shows the averaged spectrum for

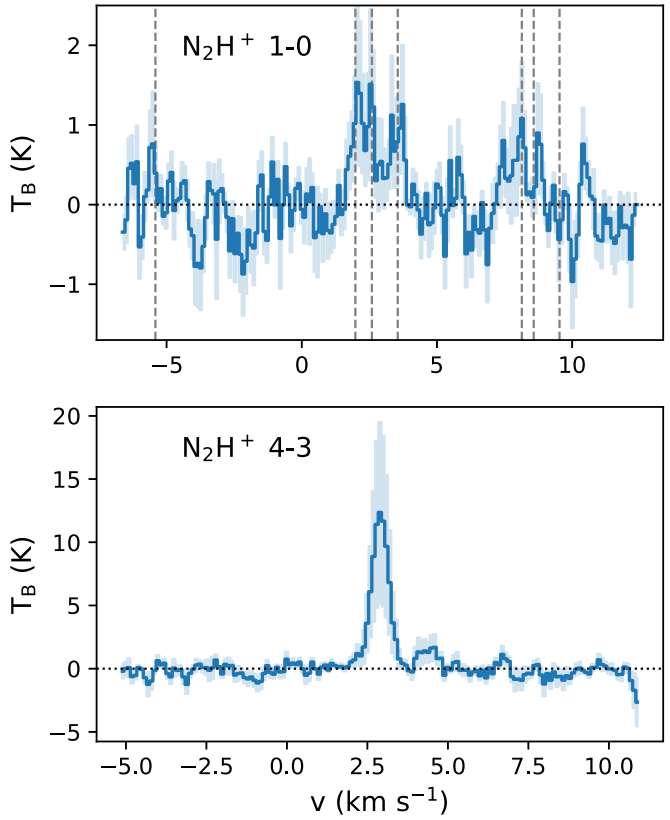

Figure 1. Spectra for the N_2H^+ $J = 1$–0 (top) and $J = 4$–3 (bottom) lines after de-projection, stacking, and averaging over a ring from $0\farcs8$ to $2''$. Light shading indicates the 1σ uncertainty in each channel. Vertical dashed lines show the expected location of the 1–0 hyperfine lines.

a ring from $0\farcs8$ to $2''$ as well as the ring-averaged 4–3 spectrum for the same parameters.

Multiple hyperfine lines are clearly seen in the averaged 1–0 spectrum. Given sufficient S/N, the relative strengths of the different hyperfine components can be used to measure the optical depth (e.g., Mangum & Shirley 2015). We use the ratio of the $1_{2,3}$–$0_{1,2}$ line relative to the four next strongest hyperfine lines as they appear in our averaged spectrum to calculate the optical depth. For each ratio our data gives an optical depth greater than 1, ranging from 1.5 for the $1_{2,2}$–$0_{1,1}$ line to 66 for the $1_{2,1}$–$0_{1,1}$ line. If the N_2H^+ 1–0 emission is indeed optically thick, the beam temperature should be roughly equal to the gas temperature, implying that N_2H^+ is emitting from gas colder than 2 K. As we discuss below, this seems unlikely given our current understanding of the physical conditions within the TW Hya disk. A more likely explanation is that the S/N remains too poor to use the relative strength of the hyperfine components to constrain the optical depth.

The ring-averaged peak brightness temperatures of the 1–0 and 4–3 lines are 1.5 ± 1 K and 12 ± 7 K, respectively, where the uncertainty is the 1σ value. N_2H^+ is posited to emit at temperatures close to the CO freeze-out temperature. At the relevant radii in TW Hya the freeze-out temperature is expected to be 21 K (see Schwarz et al. 2016). These brightness temperatures are well below this value, and thus the emission is assumed to be optically thin. Radial variations in the intensity of the 4–3 line within our annular bins likely contribute to the uncertainty for the ring-averaged peak brightness. However, as we are directly comparing the 4–3 data to the 1–0 data, we choose to treat the two data sets in the same way when averaging. Assuming local thermodynamic equilibrium, the ratio of the integrated intensities can be used to measure the excitation temperature (Goldsmith & Langer 1999):

$$\frac{\nu_u^2 A_l I_u}{\nu_l^2 A_u I_l} = \frac{g_u}{g_l} e^{-E_{ul}/kT} \quad (1)$$

where ν is the line frequency, A is the Einstein coefficient, I is the integrated intensity, g is the statistical weight for a linear rotor, E_{ul} is the energy difference between the two transitions, k is the Boltzmann constant, and T is the excitation temperature. Integrating the ring-summed spectrum for each transition gives an integrated intensity (and 1σ uncertainty) of 5.1 ± 0.2 K km s^{-1} for the 1–0 transition, and 28.7 ± 0.8 K km s^{-1} for the 4–3 transition. Using these values we find an excitation temperature of 39 K, with a 1σ uncertainty of 2 K.

4. Discussion

At the radii we consider, $0\farcs8$–$2''$, the radial temperature profile based on observations of ^{13}CO is roughly constant at 21 K (Schwarz et al. 2016). That the temperature probed by ^{13}CO remains constant over many radii suggests that the ^{13}CO emission is originating primarily from just above the CO snow surface. This can also be seen for the more inclined IM Lup disk, where the CO snow surface is directly imaged in addition to constraining the CO freeze-out temperature to ~21 K (Pinte et al. 2018). As such the 21 K from ^{13}CO provides an upper limit for the midplane temperature at these radii. This is consistent with models of the TW Hya disk (e.g., Du et al. 2015; Kama et al. 2016), which set the midplane temperature in this region at temperatures between 10 and 20 K. Thus, the 39 ± 2 K gas where N_2H^+ is emitting resides above the midplane.

In the disk models of Aikawa et al. (2015) and van't Hoff et al. (2017; itself based on the Kama et al. 2016 model), which focus specifically on the N_2H^+ 4–3 emission, the 40 K gas temperature contour is at a scale height of $z/r \approx 0.2$ for the radii where N_2H^+ emission is observed. Both sets of models predict N_2H^+ emission at this scale height. In the Aikawa et al. (2015) models including millimeter grains, CO has been converted to CO_2 ice at a scale height of 0.2, while photodissociation prevents N_2 from being reprocessed into NH_3 ice. This combination of a low CO abundance and a high N_2 abundance results in a layer of N_2H^+. CO_2 ice has been proposed as a potential reservoir of volatile carbon in disks such as TW Hya with a low CO gas abundance (Eistrup et al. 2016; Bosman et al. 2018; Schwarz et al. 2018). It is also worth noting that our derived temperature for the N_2H^+ emitting layer of 39 ± 2 K is close to the expected desorption temperature of CO_2 ice.

Alternatively, in the van't Hoff et al. (2017) model a surface layer of N_2H^+ is generated when CO has been dissociated by ultraviolet photons while N_2 remains self-shielded. These models are specifically tailored to TW Hya while considering only a small network of chemical reactions. The best fit to the observed N_2H^+ 4–3 emission in TW Hya occurs when both the CO and N_2 gas abundances have been reduced, with a total N_2/CO ratio of 1. In summary, there are a variety of factors that influence the morphology of the N_2H^+ emission in TW Hya, with photodissociation and the CO and N_2 gas abundances being of particular importance. While several

combinations of processes match the observed emission, it is clear that in this system N_2H^+ emission is not a good tracer of the CO snowline deeper in the disk. That the N_2H^+ emission in TW Hya originates from a surface layer was also suggested by Nomura et al. (2016) based on the observed brightness temperature of the 4–3 line.

5. Summary

We use averaged observations of the N_2H^+ $J = 1$–0 and $J = 4$–3 lines from $0\farcs8$ to $2''$ in TW Hya to derive the temperature of the N_2H^+ emitting layer. We find an excitation temperature of 39 K with a 1σ uncertainty of 2 K, significantly warmer than the expected midplane temperature of $<$20 K at the radii where N_2H^+ is observed to emit. Therefore, we conclude that in TW Hya N_2H^+ primarily emits from a surface layer, with the vertical boundaries set by processes such as photodissociation or chemical reprocessing, rather than a layer deeper in the disk bounded by the direct freeze-out of N_2 and CO. These results highlight the importance of understanding protoplanetary disk structure when interpreting molecular line observations.

This Letter makes use of the following ALMA data: JAO. ALMA#2011.0.00340.S and JAO.ALMA #2016.0.00592.S. ALMA is a partnership of European Southern Observatory (ESO) (representing its member states), National Science Foundation (USA), and National Institutes of Natural Sciences (Japan), together with National Research Council (Canada), National Science Council and Academia Sinica Institute of Astronomy and Astrophysics (Taiwan), and Korea Astronomy and Space Science Institute (Korea), in cooperation with Chile. The Joint ALMA Observatory is operated by ESO, Associated Universities, Inc/National Radio Astronomy Observatory (NRAO), and National Astronomical Observatory of Japan. The National Radio Astronomy Observatory is a facility of the National Science Foundation operated under cooperative agreement by Associated Universities, Inc. This work was supported by funding from NSF grant AST-1514670 and NASA NNX16AB48G. K.S. acknowledges the support of NASA through Hubble Fellowship Program grant *HST*-HF2-51419.001, awarded by the Space Telescope Science Institute, which is operated by the Association of Universities for Research in Astronomy, Inc., for NASA, under contract NAS5-26555.

Facility: ALMA.

Software: CASA v4.7.0 (McMullin et al. 2007), eddy (Teague 2019), matplotlib (Hunter 2007), numpy (van der Walt et al. 2011).

ORCID iDs

Kamber R. Schwarz https://orcid.org/0000-0002-6429-9457
Richard Teague https://orcid.org/0000-0003-1534-5186
Edwin A. Bergin https://orcid.org/0000-0003-4179-6394

References

Aikawa, Y., Furuya, K., Nomura, H., & Qi, C. 2015, ApJ, 807, 120
Bosman, A. D., Walsh, C., & van Dishoeck, E. F. 2018, A&A, 618, A182
Du, F., Bergin, E. A., & Hogerheijde, M. R. 2015, ApJL, 807, L32
Eistrup, C., Walsh, C., & van Dishoeck, E. F. 2016, A&A, 595, A83
Goldsmith, P. F., & Langer, W. D. 1999, ApJ, 517, 209
Hunter, J. D. 2007, CSE, 9, 90
Kama, M., Bruderer, S., van Dishoeck, E. F., et al. 2016, A&A, 592, A83
Kastner, J. H., Qi, C., Dickson-Vandervelde, D. A., et al. 2018, ApJ, 863, 106
Mangum, J. G., & Shirley, Y. L. 2015, PASP, 127, 266
McMullin, J. P., Waters, B., Schiebel, D., Young, W., & Golap, K. 2007, in ASP Conf. Ser. 376, Astronomical Data Analysis Software and Systems XVI, ed. R. A. Shaw, F. Hill, & D. J. Bell (San Francisco, CA: ASP), 127
Nomura, H., Tsukagoshi, T., Kawabe, R., et al. 2016, ApJL, 819, L7
Pinte, C., Ménard, F., Duchêne, G., et al. 2018, A&A, 609, A47
Qi, C., Öberg, K. I., Andrews, S. M., et al. 2015, ApJ, 813, 128
Qi, C., Öberg, K. I., Wilner, D. J., et al. 2013, Sci, 341, 630
Schwarz, K. R., Bergin, E. A., Cleeves, L. I., et al. 2016, ApJ, 823, 91
Schwarz, K. R., Bergin, E. A., Cleeves, L. I., et al. 2018, ApJ, 856, 85
Teague, R. 2019, JOSS, 4, 1220
Teague, R., Henning, T., Guilloteau, S., et al. 2018, ApJ, 864, 133
van't Hoff, M. L. R., Walsh, C., Kama, M., Facchini, S., & van Dishoeck, E. F. 2017, A&A, 599, A101
van der Walt, S., Colbert, S. C., & Varoquaux, G. 2011, CSE, 13, 22
Yen, H.-W., Koch, P. M., Liu, H. B., et al. 2016, ApJ, 832, 204
Zhang, K., Bergin, E. A., Blake, G. A., et al. 2016, ApJL, 818, L16